Spectroscopic evidence for engineered hadronic bound state formation in repulsive fermionic SU(N) Hubbard systems

Miklós Antal Werner,[1,2,3] Cătălin Paşcu Moca,[2,4] Márton Kormos,[1,2] Örs Legeza,[3,5] Balázs Dóra,[1,6] and Gergely Zaránd[1,2]

[1]*Department of Theoretical Physics, Institute of Physics, Budapest University of Technology and Economics, Műegyetem rkp. 3. H-1111 Budapest, Hungary*

[2]*MTA-BME Quantum Dynamics and Correlations Research Group, Budapest University of Technology and Economics, Műegyetem rkp. 3. H-1111 Budapest, Hungary*

[3]*Strongly Correlated Systems Lendület Research Group, Wigner Research Centre for Physics, P.O. Box 49, 1525 Budapest, Hungary*

[4]*Department of Physics, University of Oradea, 410087, Oradea, Romania*

[5]*Institute for Advanced Study, Technical University of Munich, Lichtenbergstrasse 2a, 85748 Garching, Germany*

[6]*MTA-BME Lendület Topology and Correlation Research Group, Budapest University of Technology and Economics, Műegyetem rkp. 3. H-1111 Budapest, Hungary*

(Received 29 November 2022; revised 25 July 2023; accepted 1 September 2023; published 9 October 2023)

Particle formation represents a central theme in various branches of physics, often associated to confinement. Here we show that dynamical hadron formation can be spectroscopically detected in an ultracold atomic setting within the most paradigmatic and simplest model of condensed matter physics, the repulsive SU(N) Hubbard model. By starting from an appropriately engineered high-energy initial state of the strongly interacting SU(3) Hubbard model, doublons (mesons) and trions (barions) naturally emerge during time evolution and thermalize to a negative temperature quantum gas, as demonstrated by extensive one-dimensional simulations and exact diagonalization calculations. For strong interactions, trions become heavy and attract each other strongly. Their residual interaction with doublons generates doublon diffusion, as captured by the evolution of the equal time density correlation function. Although our numerical calculations are performed on one-dimensional chains, many of our conclusions extend to a large variety of initial conditions and hold for other spatial dimensions and all SU($N > 2$) Hubbard models.

DOI: 10.1103/PhysRevResearch.5.043020

I. INTRODUCTION

Nonequilibrium dynamics have already provided us with a plethora of interesting phenomena, ranging from negative temperature states [1,2] through universal scaling across quantum phase transitions [3–6] to thermalization dynamics [7–9]. In this context, there has recently been a large surge of interest in understanding and analyzing confinement in spin chains [10–15]. Confinement is not only related to many-body localization and slow entanglement dynamics [16–18] but is also responsible for creating bound states of several interacting particles [13,19–21], plays a prominent role in quantum chromodynamics, and has a crucial role in particle formation in the early universe [22].

For the formation of bound states, confinement is, however, not crucial. Nuclei are formed by hadrons interacting via short-ranged interactions, and short-range attractive interactions also give rise to many-particle bound states in ultracold atomic systems [23,24] and are responsible for Cooper pairing [25]. Fermionic and bosonic bound states can emerge in ultracold atomic settings, which provide a fantastic platform to simulate and investigate strongly interacting forms of matter in a laboratory framework [26–29]. The hyperfine spin of fermionic atoms, in particular, can play the role of quark colors or spins in condensed matter, and thereby enables experimentalists to emulate phenomena appearing in quantum chromodynamics [30–32] in the context of hadronic matter as well as simulating SU(N) generalizations of condensed matter systems [33–40].

Attractive fermions such as ^{6}Li, e.g., have been proposed to display color superfluidity and baryon formation at sufficiently low temperatures [33,35], similar to how hadrons form in the expanding and cooling universe. Fermion gases with attractive interaction are, however, quite rare, and rather unstable against three-body losses, especially in the regime of large scattering length [41]. Moreover, cooling a fermion gas is a notoriously hard problem [26,42]. It is mostly for these reasons that the state proposed in Ref. [35] remains elusive and has not been observed so far.

Here we propose a different route to create hadronic matter; we demonstrate that a negative temperature hadronic gas of particles can be created in the presence of repulsive interactions by engineering certain very simple initial states. This must be contrasted with baryogenesis, where cooling is

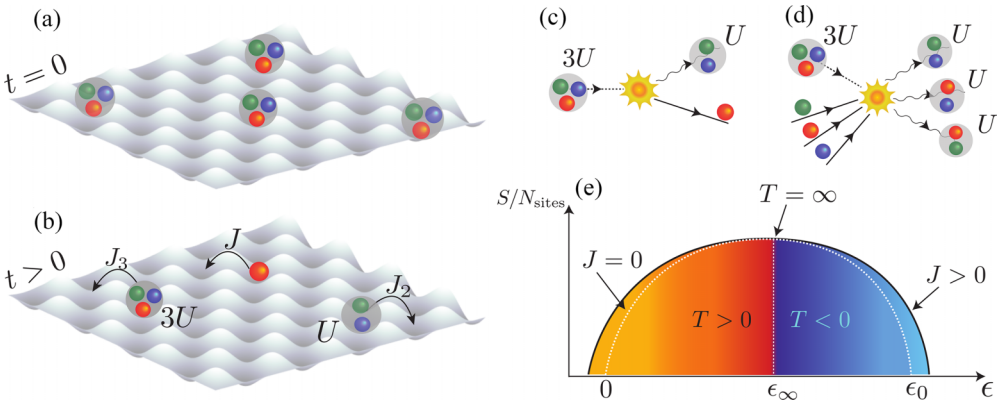

FIG. 1. (a) The initial state $|\Xi\rangle$ for $N = 3$. Sites are either empty or occupied by N fermions of different colors. (b) Schematic motion for times $t > 0$: n-particle composites move between neighboring sites with hopping J_n, and have an on-site interaction energy $Un(n-1)/2$. (c) Decay of N ions ($N = 3$ in the figure) to smaller composites is forbidden by energy conservation. (d) The lowest order decay channel for $N = 3$. A trion (baryon) and three fermions (quarks) transform into three doublons (mesons). (e) Sketch of the entropy density as a function of energy density. The white dashed line indicates the $J = 0$ limit. The entropy density has a maximum at energy density ϵ_∞, where the temperature diverges and changes signs. For states with $\epsilon < \epsilon_\infty$, the temperature is positive, while for states with $\epsilon > \epsilon_\infty$ it becomes negative.

responsible for a spontaneous formation of hadrons and confinement also plays an important role. We also demonstrate that by using quench spectroscopy, one can detect these particles unambiguously. This observation opens the door towards simulating and capturing composite particle formation with appropriately engineered initial states in a much more stable cold atomic environment. Indeed, cold atomic systems such as ^{137}Yb or ^{87}Sr are today almost routinely used to realize stable repulsive SU(N) gases [43–46] with interesting spin structures [47,48], unique thermodynamic properties [49], and prethermal states [50,51]. In an optical lattice, they realize the repulsive SU(N) Hubbard model [47,52,53],

$$H = -J \sum_{\langle \mathbf{r},\mathbf{r}'\rangle} \sum_{\alpha=1}^{N} (\psi^\dagger_{\mathbf{r}\alpha} \psi_{\mathbf{r}'\alpha} + \text{H.c.}) + \frac{U}{2} \sum_{\mathbf{r}} n_{\mathbf{r}}(n_{\mathbf{r}} - 1), \quad (1)$$

describing fermions of N different colors, $\psi^\dagger_{\mathbf{r}\alpha}$, moving around a lattice, and interacting locally via a color-independent interaction, U, with $n_{\mathbf{r}} = \sum_\alpha \psi^\dagger_{\mathbf{r}\alpha}\psi_{\mathbf{r}\alpha}$ the number of fermions at site $\mathbf{r}$.

At low temperatures, the repulsive Hubbard model hosts exotic Fermi liquid and Mott states with antiferromagnetic correlations [47,54,55], but here we focus on the structure of *high energy states* of negative temperatures, where spin correlations are not essential, and completely different physical properties emerge. The initial state which we propose to engineer is a product of N-fermion states [56,57],

$$|\Xi\rangle = \prod_{\mathbf{r}\in\Xi} \left(\prod_{\alpha=1}^{N} \psi^\dagger_{\mathbf{r}\alpha} \right) |0\rangle, \quad (2)$$

where Ξ denotes a subset of sites. As we show, this state, depicted for $N = 3$ in Fig. 1, necessarily evolves to a negative temperature state for *any* $U > 0$, but its dynamical properties change dramatically upon increasing the ratio, U/J, and for $U/J \gtrsim 1$ a strongly interacting quantum gas of trions and doublons emerges. Similar one-dimensional bosonic initial states have been investigated in Ref. [58] for $N = 2$.

II. RESULTS

A. Quench spectroscopy and resonances

The formation of composite particles can most easily be detected by quench spectroscopy [10], i.e., by analyzing the time evolution of the state Eq. (2) and its Fourier spectrum. In our numerical calculations, our primary focus lies on a one-dimensional chain of SU(3) fermions. However, we also provide results for the more commonly studied SU(2) Hubbard model, which can be found in Appendix D. We performed non-Abelian infinite chain time-evolving block decimation (NA-TEBD) simulation (see Appendix A and Refs. [59–61] for details), which we supplement by exact diagonalization calculations. Using an infinite chain algorithm protects us from finite-size effects in our dynamical simulations [62], but the rapidly growing entanglement of the quantum state sets a maximal time threshold even for the large bond dimensions accessible for our efficient non-Abelian code, $M \approx 15\,000$ [61]. In the left panel of Fig. 2, we show the time evolution of the probabilities p_n of having n fermions at a site for an initial state, where three fermions have been placed at every third site.

For $U/J \lesssim 1$, the probabilities $p_n(t)$ display damped oscillations, and the initial occupations $p_3^{(0)} = 1/3$, $p_0^{(0)} = 2/3$, and $p_1^{(0)} = p_2^{(0)} = 0$ relax to some asymptotic values, p_n^∞. The Fourier spectra of $p_n(t)$ consist of a broad band, consistent with a band of width $\approx 4J + U$ of weakly interacting fermionic excitations. In this regime, a careful analysis reveals an exponential relaxation towards a stationary state with a rate $\sim U^2/J/\hbar$ [61].

This picture changes radically for $U/J \gtrsim 2$, where the probabilities $p_n(t)$ are pinned roughly to their initial values, indicating that the probability that three particles stay together remains close to 1, $p_3(t) \approx p_3^{(0)}$. The time-averaged probabilities of having $n = 2$ or $n = 1$ fermions at a site are suppressed, but they are finite, and almost equal. Even more strikingly, small, almost undamped oscillations decorate the $p_n(t)$ curves. The Fourier transform of these signals reveals

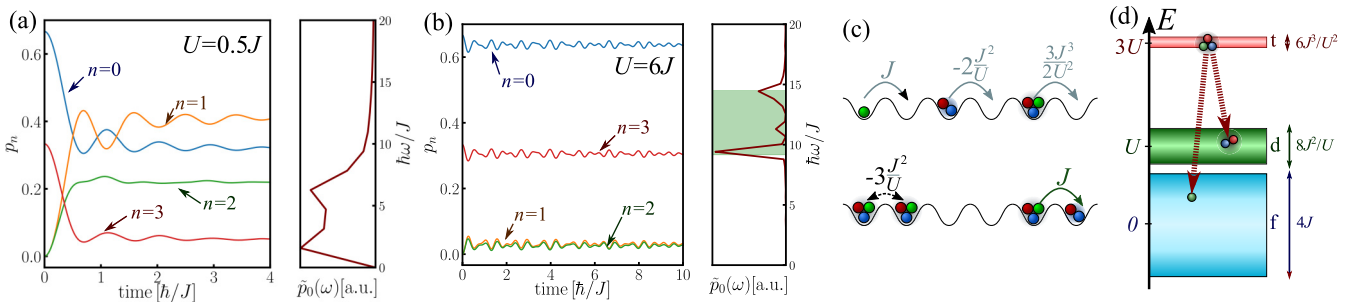

FIG. 2. (a) Evolution of the probabilities p_n for $U/J = 0.5$. The number of empty and triply occupied sites decreases rapidly, and a large fraction of sites becomes occupied by one or two fermions. The Fourier spectrum of $p_0(t)$ (right panel) consists of a spectrum of a broad frequency range up to $\hbar\omega/J \lesssim 10$. (b) Evolution of the probabilities p_n for large interaction strength, $U = 6J$. The number of empty and triply occupied sites remains almost constant apart from small oscillations. The Fourier spectrum of $p_0(t)$ is mostly restricted to a window $9.5 \lesssim \hbar\omega \lesssim 14.5$. The shading highlights the predicted spectral window, $\hbar\omega \approx 2U \pm (2J + 8J^2/U)$. Frequency peaks at the edges are due to Van Hove singularities in the single fermion (quark) band. (c) Collection of relevant energy scales in the large U limit of the SU(3) Hubbard model. In the upper part, the hopping amplitudes are shown for trions, doublons, and single fermions, while the bottom part highlights the strength of effective trion-trion interaction and the strong trion-doublon exchange process.(d) Sketch of quasiparticle energies in the large U limit. Oscillation frequencies in (b) can be interpreted as a result of coherent oscillations between a trion (baryon) and a state decomposed into a doublon (meson) and a fermion.

high-energy spectral features around $\hbar\omega \approx 2U$ [see Fig. 2(b)]. As we demonstrate, the observed oscillations of $p_n(t)$ can be understood as a result of *quantum oscillations* between *baryonic* trion states which transform coherently into *mesonic* doublon states and single fermion states, analogous to *quarks*.

B. Composite particles

In the large U limit, we can treat the hopping J as a perturbation [63,64]. Isolated n-particle states have an energy $E_n \approx Un(n-1)/2$ in this limit. Since the separation obeys $E_n - E_{n-1} = \Delta E_n = (n-1)U \gg J$, and the kinetic energy of fermions is bounded from above, these composite particles behave as quite stable entities: although they collide with each other, they can decay and transform into each other only under the condition that energy, charge, crystal momentum, and SU(N) spins are all conserved.

In the $N = 3$ case, e.g., the collision of a trion (baryon) of energy $E_3 \approx E_3^{(0)} = 3U$ with three free fermions of energy $E_1 \sim J \approx 0$ and the subsequent decay into three doublons (mesons) of energy $E_2 \approx E_2^{(0)} = U$ provides the lowest order decay channel for trions [65] [see Fig. 1(d)]. Since free fermions have a very small concentration for large U, this event is very unlikely, and trions behave as very stable composite particles. They can, however, *virtually* transform back and forth into a doublon and a fermion, and oscillate between these states at a frequency $\hbar\omega \approx E_3^{(0)} - (E_2^{(0)} + E_1^{(0)}) = 2U$. This process gives rise to the quantum oscillations observed in Fig. 2(b).

Composite particles move on the lattice with a suppressed hopping. Simple perturbation theory can be used to determine the effective hopping J_n of an n-particle composite, yielding $J_n \approx -n\,(-J)^n\,/((n-1)!\,U^{n-1})$ in all dimensions (see also Appendix B). Composite particles are therefore extremely heavy compared to fermions in the large U limit. In the case of $N = 3$, the doublon band ($n = 2$), is quite narrow compared to the band of ψ_α fermions, but the trion band ($n = 3$) is even narrower. The spectral peaks in Fig. 2(b) at $\hbar\omega \approx 2U \pm 2J$ can thus be simply understood as a result of Van Hove singularities associated with the edges of the fermion band in one-dimensional lattices [see Fig. 2(c)]. Interestingly, these spectral peaks are fully absent in the case of the usual SU(2) Hubbard model (see Appendix D), in which case coherent oscillations are also rapidly damped. This qualitative difference is caused by the fact that, for SU($N > 2$) systems, the N-particle composite breaks virtually into a $(N-1)$ ion and a single fermion, where the former still has a very small bandwidth compared to the bandwidth of fermions, while in the SU(2) model doublons break into two fermions, both with broad energy bands, in which case the effect of Van Hove singularities is reduced.

In general, we predict a resonant feature in quench spectroscopy at around $\omega \approx (N-1)U/\hbar$ in any dimension, but the precise structure of the resonance depends on dimensionality and also on lattice geometry. For $N = 3$ and a $D =$ 2-dimensional square lattice, e.g., a resonant peak is expected at $\omega \approx 2U/\hbar$, corresponding to the Van Hove singularity of the $D = 2$-dimensional lattice, while in higher dimensions broader features are expected.

C. Effective theory

The emergent composite particles interact very strongly. In the large U limit, heavy N ions dominate, and the density of other composite particles is suppressed. The energy of N ions is increased compared to its $J = 0$ value by an amount of $\delta E_N \approx zN\frac{J^2}{(N-1)U}$ due to quantum fluctuations, where one of the N fermions jumps virtually to one of the z neighboring lattice sites. Placing two N ions next to each other suppresses these quantum fluctuations and gives rise to an *attractive* interaction, $V \approx -2NJ^2/[(N-1)\,U]$. These processes are schematically illustrated in Fig. 2(c) (for the derivation, see Appendix B).

Introducing the operator $\Phi_{\mathbf{r}}^\dagger$, creating a N ion at site $\mathbf{r}$, we arrive at the following effective Hamiltonian in the large

U limit:

$$H_{\text{eff}} = -J_N \sum_{(\mathbf{r},\mathbf{r}')} (\Phi^\dagger_{\mathbf{r}} \Phi_{\mathbf{r}'} + \text{H.c.}) + E_N \sum_{\mathbf{r}} \Phi^\dagger_{\mathbf{r}} \Phi_{\mathbf{r}} - |V| \sum_{(\mathbf{r},\mathbf{r}')} n^\Phi_{\mathbf{r}} n^\Phi_{\mathbf{r}'}, \quad (3)$$

with $n^\Phi_{\mathbf{r}} = \Phi^\dagger_{\mathbf{r}} \Phi_{\mathbf{r}}$ the N-ion number operator. We note that $\Phi^\dagger_{\mathbf{r}}$ is almost equal to the product of N fermion creation operators of different colors, but quantum fluctuations dress the N ion, and mix in states where it is virtually decomposed to a set of smaller n ions. Note that for N odd, the Φ particles are fermions, while for N even they are hard-core bosons. Also note that $|V/J_N| \sim (U/J)^{N-2}$, implying that N-ion–N-ion interactions become strong for any $N > 2$ for $U \gg J$. Therefore, in the $U/J \to \infty$ limit, a gas of spinless, strongly interacting Φ particles is recovered. For $N = 3$, in particular, these particles are dynamically bound fermions, analogous to baryons in QCD.

The case $N = 2$ is somewhat specific. As discussed in Appendix D, in this case, $|V/J_2| \to 1$ as $U \to \infty$, and interacting Fermi liquid forms. In one dimension, in particular, the emerging effective Hamiltonian is equivalent to the ferromagnetic Heisenberg model.

Although the concentration of other particles is suppressed in the large U limit, their presence is still essential. In particular, the concentration p_{N-1} of $(N-1)$-ions is non-negligible, $\sim J^2/U^2$. These composite particles are created by the operators $\Theta^\dagger_{\bar{\alpha}}$, where α refers to the color of the missing fermion in the $(N-1)$ ion. Being labeled by the color of a missing SU(N) fermion, it is easy to see that $(N-1)$ ions transform according to the conjugate representation of the fundamental representation of SU(N). Although somewhat lighter than N ions, $(N-1)$ ions are also very heavy, and their interaction with the N ions is even stronger than the N-ion–N-ion interaction, V: neighboring $\Theta_{\bar{\alpha}}$ and Φ particles can exchange an α fermion in a leading order process, yielding the effective interaction term in the Hamiltonian

$$H_{\Phi-\Theta} \approx -J \sum_{(\mathbf{r},\mathbf{r}'),\,\bar{\alpha}} (\Phi^\dagger_{\mathbf{r}} \Phi_{\mathbf{r}'} \Theta^\dagger_{\mathbf{r}\bar{\alpha}} \Theta_{\mathbf{r}'\bar{\alpha}} + \text{H.c.}). \quad (4)$$

It is this interaction that is ultimately responsible for the motion and transport of $(N-1)$ ions, which, as we demonstrate later, dominates mass diffusion on the background of almost immobile N-ions.

D. Negative temperature state

We now prove that the initial state Eq. (2) must thermalize to a negative temperature state for any set Ξ, in any particle-hole symmetrical lattice, and arbitrary repulsive interaction. To prove this, we only need show that the energy density of the state $|\Xi\rangle$, $\epsilon_0 \equiv \langle\Xi|H|\Xi\rangle/N_{\text{sites}}$ is larger than that of the infinite temperature state, $\epsilon_\infty \equiv \langle H\rangle_{T=\infty}/N_{\text{sites}}$. For simplicity, we assume a particle-hole symmetrical band, but the proof carries over to any lattice and any dimension. For any product state of the form Eq. (2), the hopping part in Eq. (1) averages to zero, $\langle\Xi|H_J|\Xi\rangle = 0$, and one obtains $\epsilon_0 = \nu\, U\, N(N-1)/2$, with ν the filling factor, i.e., the ratio of sites occupied by N ions.

In the infinite temperature limit, the hopping part of the Hamiltonian also averages to zero in the case of particle-hole symmetrical Hamiltonian. The interaction part can be averaged by observing that each α fermion state at a given site is occupied with probability ν. Thus, the interaction averages to $U \sum_{\alpha<\beta} \langle n_\alpha n_\beta\rangle_{T\to\infty} = U\nu^2 N(N-1)/2$, yielding $\epsilon_\infty = \nu\,\epsilon_0 < \epsilon_0$. The latter inequality immediately implies that if the state $|\Xi\rangle$ thermalizes, it must thermalize to a negative temperature state [1,66,67] [see Fig. 1(e)].

To verify the thermalization of the system [68], we have performed exact diagonalization on small chains of sizes, $L = 12$, $L = 9$, and $L = 6$, and extracted the effective temperature using the condition that the energy density of the thermal state, $\langle H_L\rangle_T/L$, be equal to the energy density of the initial state, ϵ_0 (see Appendix C for details.) We then used the extracted negative temperature to evaluate $\langle p_n\rangle_T$, and compared the predicted values with the asymptotic values determined from our simulations.

Figure 3(a) shows the extracted inverse negative temperatures for all three system sizes as well as their $L \to \infty$ extrapolation. For small interactions, a perturbative calculation in U yields $k_B T_{\text{eff}} \propto -J^2/U$, while for large U we obtain $k_B T_{\text{eff}} \propto -U/\ln(U/J)$ (for details, see Appendix C). The agreement for weak interactions is excellent and is also very good for large U, although there an overall prefactor is employed.

The probabilities $\langle p_n\rangle_{T_{\text{eff}}}$ agree very well with the dynamically determined values, thereby evidencing the relaxation to a thermal, negative temperature state. The extracted negative temperatures correspond to very "hot" states of the system ($|k_B T| \gtrsim J$). In such large magnitude negative temperatures, eigenstates with energies much below the upper edge of the spectrum are excited. Low-energy properties [69,70] that characterize the spectrum near the edge are therefore insufficient to describe the rich dynamics that simulations uncover.

E. Entropy growth and correlations

The emergence of slow, composite particles is clearly visible in the time evolution of von Neumann entropy. The initial state at time $t = 0$ is a product state and has vanishing entanglement entropy wherever we cut the system in two. Entropy is generated by particles or excitations traveling from one part of the system to another [71]. As shown in Fig. 3(c), in our one-dimensional simulations, the von Neumann entropy increases linearly with time and the entropy growth is barely influenced by the interactions as long as $U \lesssim J$. For $U \gtrsim J$, however, the entropy growth is rapidly suppressed, indicating that (composite) particles carrying the entanglement move very slowly. Similar results are found for the SU(2) Hubbard model (see Appendix D). The linear-in-time entropy growth is expected to be a general feature even in nonintegrable models, which thermalize in the long-time limit [72] and do not exhibit many-body localization.

The dynamics of composite particles is more directly captured through time-dependent charge oscillations in Fig. 4. For small interactions, $U \lesssim J$, the charge at the origin $x = 0$, $\langle n_{x=0}(t)\rangle$ exhibits weakly damped coherent oscillations with a frequency $\sim J$, shown in Fig. 4(a). This picture changes entirely once we enter the regime $U \gtrsim J$; there, charge

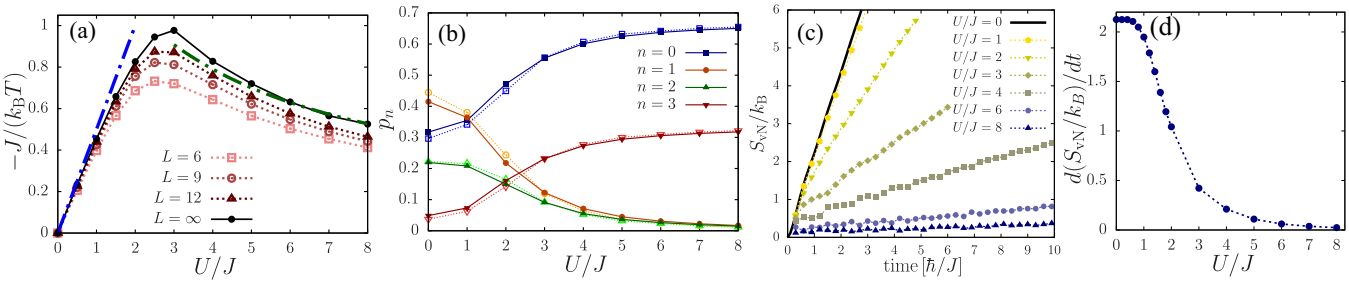

FIG. 3. (a) Extracted dimensionless inverse negative temperature $-J/T/k_B$ of the stationary state as a function of the interaction strength, U/J, as obtained for small SU(3) chains of lengths $L \in \{6, 9, 12\}$ and filling $\nu = 1/3$. Finite-size scaling extrapolation the thermodynamic ($L \to \infty$) limit is shown by black continuous line. The fitted value of $-J/T/k_B$ has a clear maximum around $U/J \approx 3$. The extracted temperature is negative for any repulsive interaction U. For small U, we obtain $k_B T \approx -2J^2/U$, while for large U, a falloff $k_B T \propto -U/\ln(U/J)$ is analytically predicted, and these limits are shown by blue and green dashed-dotted curves, respectively. (b) Stationary (long-time) charge distribution p_n as a function of the interaction strength. Filled symbols represent data obtained from NA-TEBD simulations by calculating the time average of $p_n(t)$ for long times. Thermal predictions for a short chain of length $L = 9$ are shown by empty symbols. (c) Evolution of the von Neumann entropy of a half chain for different interaction strengths. We observe linear growth of entropy for all values of U but the growth rate is strongly reduced for large U values. (d) Growth rate of the half chain entropy as a function of U/J.

oscillations slow down and universal oscillations with a frequency $\hbar\omega \sim J^3/U^2$ appear. Interestingly, these oscillations are *different* from simple composite fermion oscillations. Rather, our direct simulations with the Hamiltonian Eq. (3) show that for large U/J, $\langle n_0(t)\rangle$ approaches a universal curve described by Eq. (3) with infinitely strong interaction, $|V| \to \infty$ [see inset of Fig. 4(b)]. As discussed earlier, the SU(2) model behaves differently. There, the doublon-doublon interaction is equal to the renormalized hopping in the large U limit, and the dynamics of bosonic doublons is captured by the ferromagnetic spin 1/2 Heisenberg model (see Appendix D).

Equal time density-density correlations [73], $C_{nn}(x,t) \equiv \langle n_y(t) n_{x+y}(t)\rangle - \langle n_y(t)\rangle\langle n_{x+y}(t)\rangle$, exhibit an even more interesting picture. In the ψ_α fermion-dominated $U \lesssim J$ regime, a ballistic front propagation and a light-cone structure with slope $\propto 4J/\hbar$, i.e., twice the maximal velocity of free fermions, is observed [74] in Fig. 4(c). In contrast, for $U \gtrsim J$, the ballistic front is suppressed and $C_{nn}(x,t)$ consists of two distinct features [see Fig. 4(d)]. A large peak associated with heavy and hardly moving trions is observed at $x \approx 0$. In addition, a diffusive correlation profile appears for $x \not\approx 0$, very well described by the expression

$$|C_{nn}(x,t)| \propto \exp\left(-\frac{x^2}{4tD}\right) \tag{5}$$

in one dimension. The diffusion constant can be directly extracted from the numerical data, and it scales as

$$D \propto J^2/U. \tag{6}$$

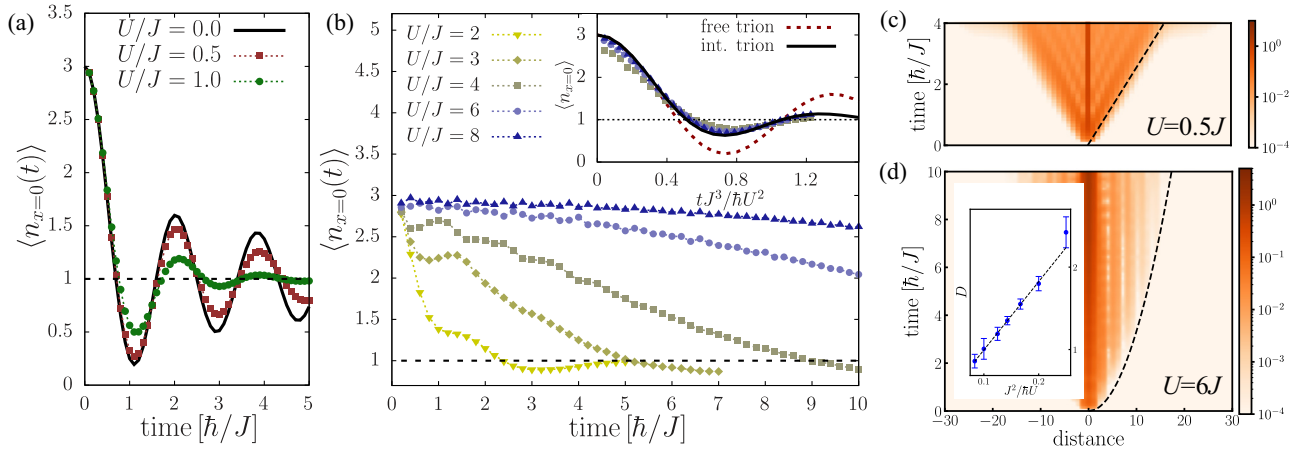

FIG. 4. Postquench dynamics starting from the initial state $|\Xi\rangle$ having triple occupancies at every third site in the one-dimensional SU(3) Hubbard chain. (a) Average fermion number at an initially triply occupied site as a function of time for weak interactions, $U/J \leqslant 1$. In the noninteracting limit, we observe algebraically decaying oscillations, which become weakly but exponentially damped for weak interactions. (b) Strong interactions, $U/J \gtrsim 1$, slow down the dynamics. Inset: The rescaled curves, $\langle n_{x=0}(t\,J^3/U^2/\hbar)\rangle$, collapse to a single universal curve for $U \to \infty$, well captured by the $|V| \to \infty$ limit of the effective Hamiltonian Eq. (3) (continuous line). (c) Amplitude of equal time density-density correlations $|C_{nn}(x,t)|$ for $U = 0.5J$. Correlations develop within a light cone of a slope $\propto 4J/\hbar$, i.e., twice the maximal velocity of free fermions. (d) Amplitude of equal time density-density correlations for strong interaction, $U = 6J$, where distance is measured in the lattice constant. Apart from the central trion peak at zero distance, correlations spread diffusively according to Eq. (5). Inset: The fitted diffusion constant D scales as $D \sim J^2/U$, evidencing meson (doublon) diffusion.

This scaling is clearly related to the doublon diffusion. Doublons have a small and non-negligible concentration and move much faster than trions. They collide with the background trions after a collision time $\tau \sim \hbar U/J^2$, and propagate diffusively due to these collisions with a diffusion constant $D \propto J^2/U/\nu^2$ [see inset of Fig. 4(d)].

The one-dimensional SU(2) Hubbard model is again an exception because it is integrable for any interaction strength, in contrast to SU($N > 2$) Hubbard models, which are integrable only in certain limits. Due to integrability, equal time charge-charge correlations remain ballistic for strong interactions, as dictated by generalized hydrodynamics [74]. The presence of ballistic two-fermion bound states appears as a double light cone structure in the correlator (see Appendix D for details). While ballistic transport is generally expected for integrable systems, it is worth noting that for some perturbed (almost) infinite temperature initial states, superdiffusive behavior has been observed [75–78].

III. DISCUSSION

In the previous sections, we have shown that hadronlike bound states can be engineered very easily in optical lattices: one just has to prepare an initial state, where SU(N) fermions are placed in N-fermion groups to a subset of lattice sites. A repulsive interaction $U \gtrsim J$ stabilizes composite particles in this case, and bound states and resonances of a hadronic nature emerge dynamically as a result of strong interactions. These heavy composite particles are simply stabilized by conservation laws, especially by that of energy and charge conservation, and form a hadron gas of strongly interacting bosons and fermions [56,57,79]. Signatures of the aforementioned composite particles appear clearly in quench spectroscopy as well as dynamical correlation functions (structure factors), which also reveal–although indirectly—the nature of their interaction.

In the particular case of $N = 3$, the heaviest bound states are trions (baryons), while composites of two particles behave as somewhat lighter mesons (doublons), in analogy with QCD. The original, bare ψ_α fermions play the role of quarks in this picture.

There are, however, many important differences between our cold atomic system and QCD: While single fermions are well-defined quasiparticles in the Hubbard model, confinement in QCD prevents the presence of lone quarks. Also, mesons in QCD are color neutral quark-antiquark pairs, while doublons in the SU(3) Hubbard model have a color, and transform nontrivially under SU(3) symmetry. Finally, hadrons form spontaneously in the expanding universe, while we propose to engineer a very high-energy (negative temperature) state, where bound three-particle states are abundant and are stabilized by a strong repulsive interaction.

Similarly, a rich picture emerges for larger values of N, where n ions with $n = 1, \ldots, N$ exist and become long-lived particles for $U \gg J$. These particles behave somewhat similarly to resonances in particle physics: They can transform into each other via many-particle collisions and their densities equilibrate with time to form a negative temperature gas of hadronlike bound states. Notice, however, that since the emergent composite particles are very heavy and the decay channels require many-particle collisions, thermalization takes place at timescales much longer than the characteristic time $t \sim \hbar/J$ of the bare ψ_α fermions' propagation.

We should note that the ordinary $N = 2$ Hubbard model is somewhat special, as we demonstrated extensively. In this case, a hard core bosonic doublon gas emerges for $U \gg J$ (with a small concentration of unbound fermions). However, while for $N > 3$ the effective nearest-neighbor interaction between N ions becomes infinite, for $N = 2$ the nearest-neighbor interaction between doublons remains finite compared to their kinetic energy, and their motion is described by an effective ferromagnetic SU(2) symmetrical Heisenberg model. In addition, in $D = 1$ dimension, the $N = 2$ fermionic Hubbard model is exactly solvable, and therefore particles as well as correlations spread ballistically rather than diffusively [74,78,80].

Interestingly, for bipartite lattices, one can also show in any dimension that for the states $|\Xi\rangle$, the time evolution of the density of the repulsive gas is identical to that of the attractive gas. To prove this, we note that on a bipartite lattice, the gauge transformation $\mathcal{K}: \psi_{\mathbf{r}\alpha} \to (-1)^{||\mathbf{r}||}\psi_{\mathbf{r}\alpha}$, flipping the sign of the fermion operators on one sublattice of the bipartite lattice, changes the sign of J but leaves the initial state as well as the density operator invariant, $\mathcal{K}: \; H_{J,U} \to H_{-J,U}$ and $|\Xi\rangle \to |\Xi\rangle$. Combing the time-reversal symmetry $\mathcal{T}$ with $\mathcal{K}$ then yields, $\mathcal{T}\,K\, e^{-i\,t\,H_{J,U}/\hbar}|\Xi\rangle = e^{-i\,t\,H_{J,-U}/\hbar}|\Xi\rangle$. Since both the time reversal and the gauge transformation $\mathcal{K}$ leave the density invariant, this implies that, starting from state $|\Xi\rangle$, the time evolution of density correlations is identical for U and for $-U$. Therefore, the quantum quench protocol suggested here can also be viewed as effectively realizing a gas of strongly attractive ψ fermions [66].

Let us close this paper by discussing experimental accessibility. Initial states for $N = 2$ with two fermions at every second site were realized a long time ago [56–58]. The preparation of trion states could be performed by following similar protocols, but for $N > 2$, three particle losses may become an important factor [41,81]. To decrease these losses, one should therefore use atoms with a relatively short scattering length a_s compared to the wavelength of the optical lattice, λ. This condition is satisfied by ^{173}Yb, having a scattering length $a_s \approx 10\,\text{nm}$ [39]. A simple calculation yields that the ratio of the interaction U and the three-body loss rate of a trion, γ, scales as $U/(\gamma h) \sim (\lambda/a_s)^3$. For the laser used in Ref. [39] with $\lambda = 759\,\text{nm}$, e.g., and for a barrier height corresponding to $U/J \approx 1$, we obtain the estimate $U/h = J/h \approx 300\,\text{Hz}$, while the three-body loss rate remains $\gamma \approx 0.16\,\text{Hz} \ll J/h$. The timescale of three-body losses is thus more than 10^3 times larger than that of the dynamical scale of the strongly interacting gas in the regime where trions and doublons form, and should be experimentally accessible [39,82].

Necessary measurement times and extracted quench spectra are also within reach. The basic timescale of the measurements is set by $h/U \approx 3.3\,\text{ms}$. For the data in Figs. 2(a), 2(b), 4(a), 4(c), and 4(d), this implies measurement times ranging between $1 - 30\,\text{ms}$, which seem to be within reach even in strongly interacting systems [58]. Necessary measurement times can further be reduced by a factor $\sim 2 - 3$ in one- and two-dimensional systems by increasing the

perpendicular confinement, and thereby the value of U, at the expense of increasing the three-body decay rate by a factor of $\sim 4-9$. Such a decrease of the measurement time would enable one to access the universal dynamics emerging at large U, as presented in Fig. 4(b).

Although thermal fluctuations of the cold gas prior to state preparation also lead to limitations, state-of-the-art fermionic experiments allow one to enter the small entropy (small temperature) regime [47,83] such that the span of our simulations (measurement times) is still below the thermal timescale, $\sim\hbar/k_B T$, and the fraction of entropy-generated fermions and doublons is still small.

We therefore believe that—while experiments with $N \geqslant 4$ systems may be extremely challenging–the fascinating composite particle dynamics of the emergent negative temperature hadron gas in repulsive SU(2) and SU(3) Hubbard models, discussed in this paper, is within experimental reach in all spatial dimensions.

ACKNOWLEDGMENTS

This research is supported by the National Research, Development and Innovation Office NKFIH through research Grants No. K134983, No. K138606, No. K142179, and No. SNN139581, within the Quantum National Laboratory of Hungary program (Project No. 2017-1.2.1-NKP-2017-00001). M.A.W. has also been supported by the Janos Bolyai Research Scholarship of the Hungarian Academy of Sciences and by No. ÚNKP-21-4-II and No. ÚNKP-22-5-BME-330 New National Excellence Program of the Ministry for Culture and Innovation from the source of the National Research, Development and Innovation Fund. C.P.M. acknowledges support by the Ministry of Research, Innovation and Digitization, CNCS/CCCDI-UEFISCDI, under Project No. PN-III-P4-ID-PCE-2020-0277 and the project for funding excellence, Contract No. 29 PFE/30.12.2021. O.L. acknowledges support from the Hans Fischer Senior Fellowship program funded by the Technical University of Munich–Institute for Advanced Study and from the Center for Scalable and Predictive methods for Excitation and Correlated phenomena (SPEC), funded as part of the Computational Chemical Sciences Program by the U.S. Department of Energy (DOE), Office of Science, Office of Basic Energy Sciences, Division of Chemical Sciences, Geosciences, and Biosciences at Pacific Northwest National Laboratory. We acknowledge KIFÜ for awarding us access to resources based in Hungary.

APPENDIX A: NON-ABELIAN MPS SIMULATIONS

Matrix product state (MPS) simulations have been performed for the one-dimensional Hubbard model with $N = 3$ colors. The real-time dynamics, generated by the Hamiltonian Eq. (1), has been simulated using the infinite chain non-Abelian time evolving block decimation (NA-TEBD) algorithm [61], while exploiting the full SU(3) × U(1) symmetry of the model. We have kept $M_{\text{mult}} = 2500$ multiplets in the NA-MPS, which corresponds to a usual bond dimension $M \approx 15\,000$. The time step in the second-order Suzuki-Trotter approximation was set to $J\Delta t = 0.01$. The dependence of the time-dependent average charge and half chain entropy on the bond dimension M_{mult} is shown in Fig. 5 for interaction strength $U/J = 4$. For this interaction strength, data with the two largest bond dimension values start to diverge at times $t \gtrsim 10\,\hbar/J$, which indicates the time span of our simulation. Interestingly, the average fermion number is much less sensitive to bond dimension. Similar tests have also been performed for other interaction strengths to ensure convergence of the data shown in the main text.

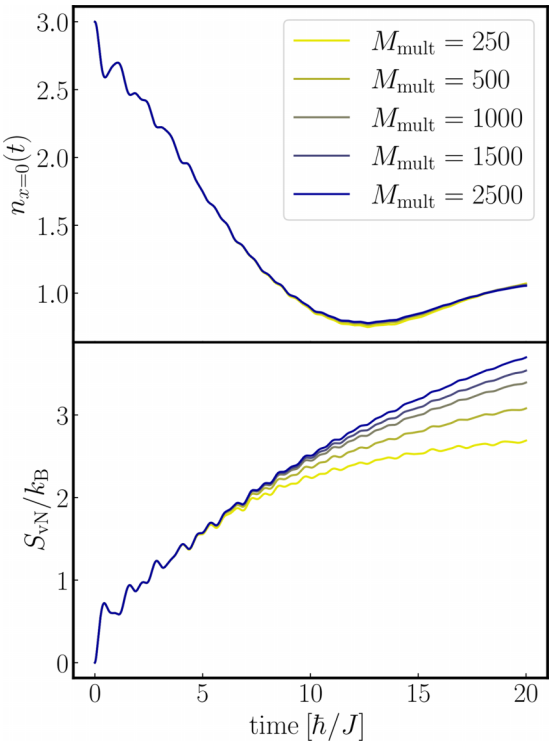

FIG. 5. Average fermion number at a triply occupied site (a) and half-chain von Neumann entropy (b) as a function of time for different multiplet bond dimensions M_{mult}. Interaction strength is set to $U/J = 4$ for both panels.

We have also performed TEBD simulations using the effective trion Hamiltonian Eq. (3) in the $|V| \to \infty$ limit, by using the residual $U(1)$ symmetry of the effective model. Since the infinitely strong interaction forbids trions from hopping next to each other, we could map the strongly interacting limit to free fermions by using a method of Cheong and Henley [84].

APPENDIX B: DERIVATION OF EFFECTIVE N-ION HAMILTONIAN

The effective Hamiltonians describing the motion of composite particles can be constructed by performing perturbation theory in J. The effective hopping for an n ion, e.g., can be estimated in leading order [63,85,86] as

$$-J_n = \langle 0| \prod_{\alpha=1}^{n} \psi_{\mathbf{r}\alpha}\, T_{\mathbf{r},\mathbf{r}'} \left(\frac{1}{E_n^{(0)} - H_U} T_{\mathbf{r},\mathbf{r}'} \right)^{n-1} \prod_{\beta=1}^{n} \psi^\dagger_{\mathbf{r}'\beta} |0\rangle,$$

where $\mathbf{r}$ and $\mathbf{r}'$ are two neighboring sites, H_U denotes the on-site energy, and $T_{\mathbf{r},\mathbf{r}'} = -J \sum_{\alpha=1}^{N} \psi^\dagger_{\mathbf{r}\alpha} \psi_{\mathbf{r}'\alpha}$ the hopping operator from $\mathbf{r}'$ and $\mathbf{r}$. In the intermediate state, where l particles are on $\mathbf{r}$ and $(n-l)$ at site $\mathbf{r}'$, the denominator can be

evaluated as $E_n^{(0)} - E_l^{(0)} - E_{n-l}^{(0)} = Un(n-l)$. The product of the denominators can therefore be evaluated as $U\ ((n-1)!)^2$, while the order in which particles are transferred between the two sites amounts in a combinatorial factor, $n!$, yielding the result in the main text.

The effective interaction of composite particles can be similarly derived. First, we determine the perturbative energy shift of a lone n-fermion composite: In a second-order process, a fermion jumps out and back, leading to an energy shift $zn\frac{J^2}{(n-1)U}$, where the zn prefactor counts the possible different back-and-forth jump processes. We note that this shift is positive for repulsive interactions. If we now place two identical n ions next to each other, some of the jump processes become forbidden due to the Pauli exclusion principle. For n ions, the number of possible jump processes for the two composites is reduced by $2n$, therefore the total energy is shifted by $-2n\frac{J^2}{(n-1)U}$ as compared to the energy of two remote n ions. This yields an effective attractive (negative) interaction between composites on neighboring sites.

APPENDIX C: ESTIMATION OF EFFECTIVE TEMPERATURE

Direct numerical method for finite chains. The effective temperature has been estimated based on the Taylor expansion of the canonical density operator $e^{-\beta\hat{H}}$ for finite SU(3) Hubbard chains of lengths up to $L = 12$. In our calculation, the number of particles of different colors has been fixed independently to $L/3$. The partition function $Z = \mathrm{Tr}e^{-\beta\hat{H}}$ and the energy density $\varepsilon = \frac{1}{ZL}\mathrm{Tr}(\hat{H}e^{-\beta\hat{H}})$ have been calculated by estimating the trace using a random pool of quantum states. In this method, the main numerical difficulty is the efficient computation of matrix-vector products, $\hat{H}|\psi\rangle$. In the SU(3) Hubbard model, we can exploit the fact that hopping terms can be applied separately for different colors, while the interaction is a diagonal operator. If we reshape the state vector $|\psi\rangle$ into a three-index tensor, where the indices stand for the subsystems of different colors, then the hopping operator is a sum of three tensor contractions where the relatively small single-color hopping operator is contracted with one of the indices of the three-index state vector. Products with the diagonal interaction operator can be even more simply evaluated by an elementwixe product of the diagonal elements and the state vector. These two tricks enabled us to reach system sizes of $L = 12$ with particle numbers (4,4,4) on a simple desktop computer, where the dimension of the relevant Hilbert space is 1.21×10^8.

Small U limit. To estimate the effective temperature for $U \ll J$, we first note that β in this limit is a very small negative number. We can therefore perform a perturbative calculation in this limit by keeping only the leading order terms in β and U and by taking the expectation value $\langle H_J + H_U\rangle_T$ with the unperturbed density operator, and equating that with the energy of the initial state. This procedure yields the equation

$$-\nu(1-\nu)\beta\int \mathrm{d}\epsilon\ \epsilon\,\rho(\epsilon) + U\tfrac{N(N-1)}{2}\nu^2 \approx \nu\ U\ \tfrac{N(N-1)}{2}, \tag{C1}$$

where $\rho(\epsilon)$ denotes the single particle density of states of the lattice. The prefactor $(1-\nu)\nu$ in the first integral is associated with the (diverging) chemical potential, $e^{-\beta\mu} \approx (1-\nu)/\nu$. On a D-dimensional cubic lattice, Eq. (C1) yields

$$\beta_{\mathrm{eff}}(U \ll J) \approx -\frac{(N-1)}{4D}\frac{U}{J^2}. \tag{C2}$$

In $D = 1$ dimension and for $N = 3$ and $\nu = 1/3$, we obtain a prefactor $1/2$, in perfect agreement with Fig. 3(a).

Large U limit. In the $U \gg J$ limit, we can consider each site as a grand canonical subsystem, weakly coupled to the rest of the system, and having a density matrix $\rho \propto e^{-\beta(Un(n-1)/2-\mu n)}$. Since N ions are abundant, the chemical potential of the subsystem must be approximately $\mu \approx U(N-1)/2$. The probability of having a single fermion is then given by $p_{n=1} \approx (1-\nu)Ne^{\beta U(N-1)/2}$, where the prefactor approximates the inverse partition function.

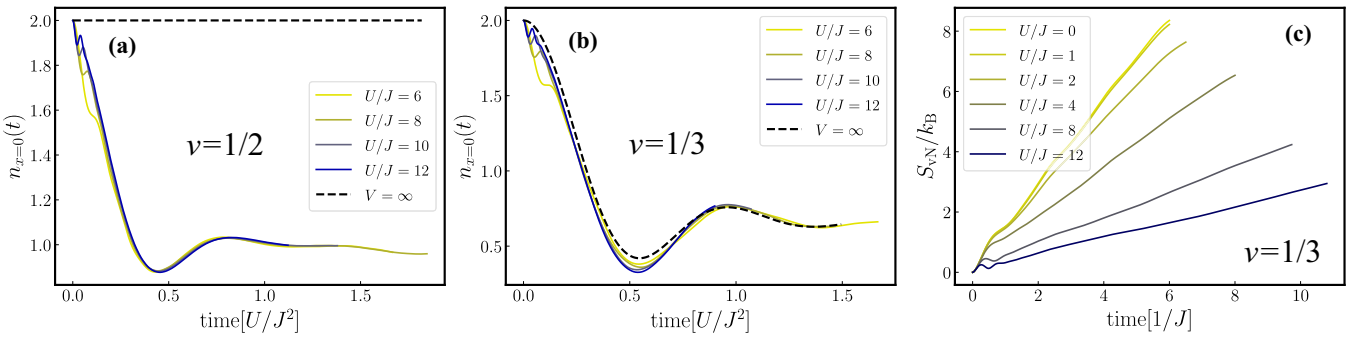

FIG. 6. (a) Average fermion number at a doubly occupied site in the SU(2) Hubbard chain as a function of time for different interaction strengths at filling $\nu = 1/2$. The unit of the time axis is set to U/J^2. Data is also shown for the effective model of doublons with infinitely strong nearest-neighbor repulsion (dashed line), in which model strong repulsion fully prevents motion of doublons at half filling. The simulated data collapse on a single nontrivial curve for different interaction strengths. (b) Average fermion number at a doubly occupied site as a function of time at filling $\nu = 1/3$. The simulated data tend to collapse on a single nontrivial curve for different interaction strengths, which differs from data generated in the infinitely repulsive effective doublon model (dashed line). (c) Evolution of the von Neumann entropy of a half chain for different interaction strengths in the SU(2) Hubbard chain. We observe linear growth of entropy for all values of U but the growth rate is strongly reduced for large U values.

The value of $p_{n=1}$ can, however, also be estimated quite simply by noticing that the state, where we have N particles at one site, say at the origin, $|N\rangle$, is not a true N-ion state at finite J/U. Quantum fluctuations allow each fermion forming the N ion to move to neighboring sites with probability amplitudes $\approx J/((N-1)U)$. This implies that a state $|N\rangle$ decomposes to a fermion and an $(N-1)$ ion with a probability $P_{N\to(N-1),1} \approx zNJ^2/[(N-1)^2U^2]$, yielding $p_1 \approx p_{N-1} \approx z\,\nu\,NJ^2/[(N-1)^2U^2]$. Comparison with the thermal average then yields

$$\beta_{\rm eff}(U \gg J) \approx -\frac{4}{(N-1)\,U}\,\ln\left(\sqrt{\frac{1-\nu}{\nu\,z}}\,\frac{(N-1)U}{J}\right), \tag{C3}$$

with $z = 2D$ on a D-dimensional cubic lattice. In the case of the third filled SU(3) chain, this theory predicts $\beta_{\rm eff} \approx -\frac{2}{U}\ln(2U)$. However, to get the precise agreement in Fig. 3(a), an overall prefactor 0.76 has also to be introduced.

APPENDIX D: SIMULATION RESULTS IN THE SU(2) HUBBARD MODEL

Here we present data for the SU(2) Hubbard model. For our numerical simulations, we consider two different initial states with specific filling factors. The first initial state has a filling factor of $\nu = 1/2$, where every second site is doubly occupied, while all other sites are empty. The second initial state has a filling factor of $\nu = 1/3$, where every third site is doubly occupied, while the rest remain empty. In the $\nu = 1/2$ case, the state is symmetric under particle-hole transformations while for the $\nu = 1/3$ filling state, particle-hole symmetry is not present. Interestingly, particle-hole symmetry seems to have no significant influence on the postquench dynamics.

In Figs. 6(a) and 6(b), the average charge of an initially doubly occupied site is shown as a function of time for $\nu = 1/2$ and $\nu = 1/3$. For strong interactions, the density of single fermion sites is negligible in the postquench state, therefore an effective theory of doublons, similar to the one presented in Sec. II C, is expected to drive the dynamics of the state. This effective theory is, however, fundamentally different from the one that emerges for $N > 2$: for $N = 2$, both the effective hopping J_2 of doublons and their effective nearest-neighbor interaction V scale as $\sim J^2/U$ in the large U limit. Therefore, in contrast to the SU($N > 2$) case, the ratio of the effective interaction strength and the effective hopping scales to unity for $U \to \infty$. The resulting effective model turns out to map on the spin $S = 1/2$ ferromagnetic Heisenberg model with an exchange coupling $\mathcal{J} \approx 4J^2/U$ as $U \to \infty$,

$$H_{\rm eff} = -\mathcal{J}\sum_{\langle \mathbf{r},\mathbf{r}'\rangle}\left(S^z_{\mathbf{r}}S^z_{\mathbf{r}'} + \frac{1}{2}(S^+_{\mathbf{r}}S^-_{\mathbf{r}'} + S^-_{\mathbf{r}}S^+_{\mathbf{r}'})\right), \tag{D1}$$

with $n_{\mathbf{r}} - 1 \leftrightarrow 2\,S^z_{\mathbf{r}}$, and the second term $\sim S^+_{\mathbf{r}}S^-_{\mathbf{r}'}$ describing the hopping of bosonic doublons. As a result, local charge oscillations are strongly damped even in the large U limit and bound state resonances are absent. The inapplicability of the $V \to \infty$ limit is demonstrated in Figs. 6(a) and 6(b), where the large U data are compared with the infinitely repulsive effective model. For filling $\nu = 1/2$, the effective model predicts a perfect freezing of the dynamics, while the simulations show a rapid equilibration to a homogeneous state, as expected in the ferromagnetic Heisenberg model. The effective model also fails for filling $\nu = 1/3$, but there the difference is not as striking as for the half-filled case.

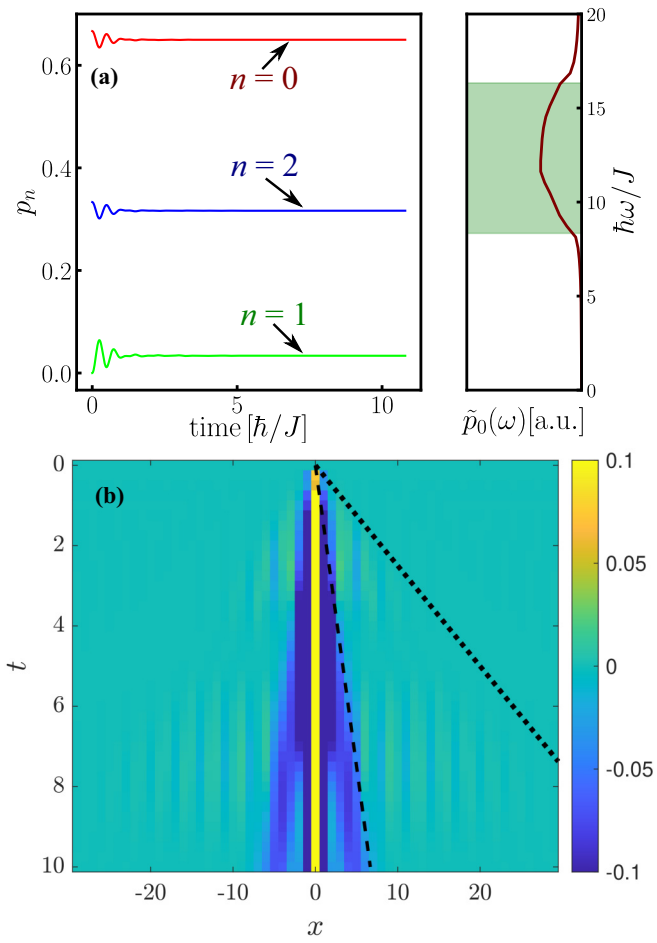

FIG. 7. (a) Evolution of the probabilities p_n in the SU(2) Hubbard-model for $U/J = 12$ and filling $\nu = 1/3$. Contrary to the SU(3) case, oscillations are damped at short times $t < \hbar/J$. The Fourier transform of $p_0(t)$ is nonzero in the frequency window $\hbar\omega \in [U-4J, U+4J]$, but no Van Hove singularity peaks are observed. (b) Equal time density-density correlations $C_n n(x,t)$ in the SU(2) Hubbard-model for $U/J = 12$ and filling $\nu = 1/3$. In contrast to the SU(3) case, correlations spread ballistically. The dotted and dashed lines correspond to velocities $4Ja/\hbar$ and $8J^2a/\hbar U$ that are twice the maximal velocities of fermions and doublons, respectively.

Figure 6(c) shows the evolution of the half-chain entropy. As expected, the entropy grows linearly as a function of time and, similarly to the SU(3) case, the entropy growth rate decreases strongly for $U/J > 1$, where the motions of doublons is responsible for entropy growth.

In Fig. 7(a), we present the results of quench spectroscopy from $p_n(t)$ for $U/J = 12$. The qualitative behavior of $p_n(t)$ is strikingly different from the SU(3) case. Oscillations are strongly damped on a timescale of $\sim\hbar/J$. The Fourier transform of $p_0(t)$ has nonzero values in the frequency window $\hbar\omega \in [U-4J, U+4J]$, corresponding to doublon $\leftrightarrow$ 2-fermion transitions, but the signal is smooth and, in contrast

to the SU(3) case, no Van Hove singularities emerge at the band edges.

Equal time density-density correlations are presented for $U/J = 12$ in Fig. 7(b). In strike contrast to the SU(3) case, they are ballistic. Two light cones are observed: one spreads by a velocity of $8J^2a/\hbar U$ that is twice the maximal velocity of the doublons, and the other, slightly visible light cone spreads by a velocity of $4J$ that is twice the maximal velocity of fermions. The reason for this difference lies in the fact that the SU(2) Hubbard model is integrable for any interaction strength, and therefore all excitations move ballistically [74], though with different velocities. In contrast, the SU($N > 2$) model is nonintegrable and excitations are expected to display diffusive behavior.

[1] S. Braun, J. P. Ronzheimer, M. Schreiber, S. S. Hodgman, T. Rom, I. Bloch, and U. Schneider, Negative absolute temperature for motional degrees of freedom, Science **339**, 52 (2013).

[2] E. Abraham and O. Penrose, Physics of negative absolute temperatures, Phys. Rev. E **95**, 012125 (2017).

[3] H. Ritsch, P. Domokos, F. Brennecke, and T. Esslinger, Cold atoms in cavity-generated dynamical optical potentials, Rev. Mod. Phys. **85**, 553 (2013).

[4] M. Gärttner, J. G. Bohnet, A. Safavi-Naini, M. L. Wall, J. J. Bollinger, and A. M. Rey, Measuring out-of-time-order correlations and multiple quantum spectra in a trapped-ion quantum magnet, Nat. Phys. **13**, 781 (2017).

[5] M. Heyl, Dynamical quantum phase transitions: A review, Rep. Prog. Phys. **81**, 054001 (2018).

[6] B. Song, S. Dutta, S. Bhave, J.-C. Yu, E. Carter, N. Cooper, and U. Schneider, Realizing discontinuous quantum phase transitions in a strongly correlated driven optical lattice, Nat. Phys. **18**, 259 (2022).

[7] M. Rigol, V. Dunjko, and M. Olshanii, Thermalization and its mechanism for generic isolated quantum systems, Nature (London) **452**, 854 (2008).

[8] J. Berges, M. P. Heller, A. Mazeliauskas, and R. Venugopalan, Qcd thermalization: *Ab initio* approaches and interdisciplinary connections, Rev. Mod. Phys. **93**, 035003 (2021).

[9] T. Langen, T. Gasenzer, and J. Schmiedmayer, Prethermalization and universal dynamics in near-integrable quantum systems, J. Stat. Mech.: Theory Exp. (2016) 064009.

[10] M. Kormos, M. Collura, G. Takács, and P. Calabrese, Real-time confinement following a quantum quench to a non-integrable model, Nat. Phys. **13**, 246 (2017).

[11] F. M. Surace and A. Lerose, Scattering of mesons in quantum simulators, New J. Phys. **23**, 062001 (2021).

[12] J. Vovrosh, H. Zhao, J. Knolle, and A. Bastianello, Confinement-induced impurity states in spin chains, Phys. Rev. B **105**, L100301 (2022).

[13] J. Vovrosh, R. Mukherjee, A. Bastianello, and J. Knolle, Dynamical hadron formation in long-range interacting quantum spin chains, PRX Quantum **3**, 040309 (2022).

[14] S. Birnkammer, A. Bastianello, and M. Knap, Prethermalization in confined spin chains, Nat. Commun. **13**, 7663 (2022).

[15] M. C. Banuls, M. P. Heller, K. Jansen, J. Knaute, and V. Svensson, A quantum information perspective on meson melting, arXiv:2206.10528.

[16] J. H. Bardarson, F. Pollmann, and J. E. Moore, Unbounded Growth of Entanglement in Models of Many-Body Localization, Phys. Rev. Lett. **109**, 017202 (2012).

[17] R. Nandkishore and D. A. Huse, Many-body localization and thermalization in quantum statistical mechanics, Annu. Rev. Condens. Matter Phys. **6**, 15 (2015).

[18] M. Brenes, M. Dalmonte, M. Heyl, and A. Scardicchio, Many-Body Localization Dynamics from Gauge Invariance, Phys. Rev. Lett. **120**, 030601 (2018).

[19] S. E. Pollack, D. Dries, and R. G. Hulet, Universality in three- and four-body bound states of ultracold atoms, Science **326**, 1683 (2009).

[20] C. H. Greene, P. Giannakeas, and J. Pérez-Ríos, Universal few-body physics and cluster formation, Rev. Mod. Phys. **89**, 035006 (2017).

[21] F. Liu, S. Whitsitt, P. Bienias, R. Lundgren, and A. V. Gorshkov, Realizing and probing baryonic excitations in Rydberg atom arrays, arXiv:2007.07258.

[22] R. Alkofer and L. von Smekal, The infrared behaviour of QCD Green's functions: Confinement, dynamical symmetry breaking, and hadrons as relativistic bound states, Phys. Rep. **353**, 281 (2001).

[23] M. W. Zwierlein, C. A. Stan, C. H. Schunck, S. M. F. Raupach, A. J. Kerman, and W. Ketterle, Condensation of Pairs of Fermionic Atoms near a Feshbach Resonance, Phys. Rev. Lett. **92**, 120403 (2004).

[24] C. Chin, M. Bartenstein, A. Altmeyer, S. Riedl, S. Jochim, J. H. Denschlag, and R. Grimm, Observation of the pairing gap in a strongly interacting Fermi gas, Science **305**, 1128 (2004).

[25] M. Randeria, J.-M. Duan, and L.-Y. Shieh, Bound States, Cooper Pairing, and Bose Condensation in Two Dimensions, Phys. Rev. Lett. **62**, 981 (1989).

[26] I. Bloch, J. Dalibard, and W. Zwerger, Many-body physics with ultracold gases, Rev. Mod. Phys. **80**, 885 (2008).

[27] S. Giorgini, L. P. Pitaevskii, and S. Stringari, Theory of ultracold atomic Fermi gases, Rev. Mod. Phys. **80**, 1215 (2008).

[28] T. Esslinger, Fermi-Hubbard physics with atoms in an optical lattice, Annu. Rev. Condens. Matter Phys. **1**, 129 (2010).

[29] X.-W. Guan, M. T. Batchelor, and C. Lee, Fermi gases in one dimension: From Bethe ansatz to experiments, Rev. Mod. Phys. **85**, 1633 (2013).

[30] M. Alford, K. Rajagopal, and F. Wilczek, QCD at finite baryon density: Nucleon droplets and color superconductivity, Phys. Lett. B **422**, 247 (1998).

[31] M. G. Alford, A. Schmitt, K. Rajagopal, and T. Schäfer, Color superconductivity in dense quark matter, Rev. Mod. Phys. **80**, 1455 (2008).

[32] J. Berges and K. Rajagopal, Color superconductivity and chiral symmetry restoration at non-zero baryon density and temperature, Nucl. Phys. B **538**, 215 (1999).

[33] C. Honerkamp and W. Hofstetter, Ultracold Fermions and the SU(N) Hubbard Model, Phys. Rev. Lett. **92**, 170403 (2004).

[34] L. He, M. Jin, and P. Zhuang, Superfluidity in a three-flavor Fermi gas with SU(3) symmetry, Phys. Rev. A **74**, 033604 (2006).
[35] A. Rapp, G. Zaránd, C. Honerkamp, and W. Hofstetter, Color Superfluidity and Baryon Formation in Ultracold Fermions, Phys. Rev. Lett. **98**, 160405 (2007).
[36] A. V. Gorshkov, M. Hermele, V. Gurarie, C. Xu, P. S. Julienne, J. Ye, P. Zoller, E. Demler, M. D. Lukin, and A. M. Rey, Two-orbital SU(N) magnetism with ultracold alkaline-earth atoms, Nat. Phys. **6**, 289 (2010).
[37] F. Scazza, C. Hofrichter, M. Höfer, P. C. De Groot, I. Bloch, and S. Fölling, Observation of two-orbital spin-exchange interactions with ultracold SU(N)-symmetric fermions, Nat. Phys. **10**, 779 (2014).
[38] M. A. Cazalilla and A. M. Rey, Ultracold Fermi gases with emergent SU(N) symmetry, Rep. Prog. Phys. **77**, 124401 (2014).
[39] C. Hofrichter, L. Riegger, F. Scazza, M. Höfer, D. R. Fernandes, I. Bloch, and S. Fölling, Direct Probing of the Mott Crossover in the SU(N) Fermi-Hubbard Model, Phys. Rev. X **6**, 021030 (2016).
[40] W. J. Chetcuti, J. Polo, A. Osterloh, P. Castorina, and L. Amico, Probe for bound states of SU(3) fermions and colour deconfinement, Commun Phys **6**, 128 (2023).
[41] J. H. Huckans, J. R. Williams, E. L. Hazlett, R. W. Stites, and K. M. O'Hara, Three-Body Recombination in a Three-State Fermi Gas with Widely Tunable Interactions, Phys. Rev. Lett. **102**, 165302 (2009).
[42] T. Fukuhara, Y. Takasu, M. Kumakura, and Y. Takahashi, Degenerate Fermi gases of Ytterbium, Phys. Rev. Lett. **98**, 030401 (2007).
[43] S. Taie, Y. Takasu, S. Sugawa, R. Yamazaki, T. Tsujimoto, R. Murakami, and Y. Takahashi, Realization of a SU(2) × SU(6) System of Fermions in a Cold Atomic Gas, Phys. Rev. Lett. **105**, 190401 (2010).
[44] S. Taie, R. Yamazaki, S. Sugawa, and Y. Takahashi, An SU(6) Mott insulator of an atomic Fermi gas realized by large-spin Pomeranchuk cooling, Nat. Phys. **8**, 825 (2012).
[45] X. Zhang, M. Bishof, S. L. Bromley, C. V. Kraus, M. S. Safronova, P. Zoller, A. M. Rey, and J. Ye, Spectroscopic observation of SU(N)-symmetric interactions in Sr orbital magnetism, Science **345**, 1467 (2014).
[46] L. Sonderhouse, C. Sanner, R. B. Hutson, A. Goban, T. Bilitewski, L. Yan, W. R. Milner, A. M. Rey, and J. Ye, Thermodynamics of a deeply degenerate SU(N)-symmetric Fermi gas, Nat. Phys. **16**, 1216 (2020).
[47] S. Taie, E. Ibarra-García-Padilla, N. Nishizawa, Y. Takasu, Y. Kuno, H.-T. Wei, R. T. Scalettar, K. R. Hazzard, and Y. Takahashi, Observation of antiferromagnetic correlations in an ultracold SU(N) Hubbard model, Nat. Phys. **18**, 1356 (2022).
[48] M. A. Perlin, D. Barberena, M. Mamaev, B. Sundar, R. J. Lewis-Swan, and A. M. Rey, Engineering infinite-range SU(N) interactions with spin-orbit-coupled fermions in an optical lattice, Phys. Rev. A **105**, 023326 (2022).
[49] E. Ibarra-García-Padilla, S. Dasgupta, H.-T. Wei, S. Taie, Y. Takahashi, R. T. Scalettar, and K. R. A. Hazzard, Universal thermodynamics of an SU(N) Fermi-Hubbard model, Phys. Rev. A **104**, 043316 (2021).
[50] C.-H. Huang, Y. Takasu, Y. Takahashi, and M. A. Cazalilla, Suppression and control of prethermalization in multicomponent Fermi gases following a quantum quench, Phys. Rev. A **101**, 053620 (2020).
[51] M. Mamaev, T. Bilitewski, B. Sundar, and A. M. Rey, Resonant dynamics of strongly interacting SU(N) fermionic atoms in a synthetic flux ladder, PRX Quantum **3**, 030328 (2022).
[52] T. Ulbricht, R. A. Molina, R. Thomale, and P. Schmitteckert, Color-charge separation in trapped SU(3) fermionic atoms, Phys. Rev. A **82**, 011603(R) (2010).
[53] O. Dutta, M. Gajda, P. Hauke, M. Lewenstein, D.-S. Lühmann, B. A. Malomed, T. Sowiński, and J. Zakrzewski, Non-standard Hubbard models in optical lattices: A review, Rep. Prog. Phys. **78**, 066001 (2015).
[54] M. Boll, T. A. Hilker, G. Salomon, A. Omran, J. Nespolo, L. Pollet, I. Bloch, and C. Gross, Spin- and density-resolved microscopy of antiferromagnetic correlations in Fermi-Hubbard chains, Science **353**, 1257 (2016).
[55] A. Mazurenko, C. Chiu, and G. Ji, A cold-atom Fermi-Hubbard antiferromagnet, Nature (London) **545**, 462 (2017).
[56] K. Winkler, G. Thalhammer, F. Lang, R. Grimm, J. Hecker Denschlag, A. J. Daley, A. Kantian, H. P. Büchler, and P. Zoller, Repulsively bound atom pairs in an optical lattice, Nature (London) **441**, 853 (2006).
[57] Y.-M. Wang and J.-Q. Liang, Repulsive bound-atom pairs in an optical lattice with two-body interaction of nearest neighbors, Phys. Rev. A **81**, 045601 (2010).
[58] S. Trotzky, Y.-A. Chen, A. Flesch, I. P. McCulloch, U. Schollwöck, J. Eisert, and I. Bloch, Probing the relaxation towards equilibrium in an isolated strongly correlated one-dimensional Bose gas, Nat. Phys. **8**, 325 (2012).
[59] G. Vidal, Efficient Simulation of One-Dimensional Quantum Many-Body Systems, Phys. Rev. Lett. **93**, 040502 (2004).
[60] G. Vidal, Classical Simulation of Infinite-Size Quantum Lattice Systems in One Spatial Dimension, Phys. Rev. Lett. **98**, 070201 (2007).
[61] M. A. Werner, C. P. Moca, O. Legeza, and G. Zaránd, Quantum quench and charge oscillations in the SU(3) Hubbard model: A test of time evolving block decimation with general non-Abelian symmetries, Phys. Rev. B **102**, 155108 (2020).
[62] Z. Wang, M. Foss-Feig, and K. R. A. Hazzard, Bounding the finite-size error of quantum many-body dynamics simulations, Phys. Rev. Res. **3**, L032047 (2021).
[63] M. Takahashi, Half-filled Hubbard model at low temperature, J. Phys. C **10**, 1289 (1977).
[64] V. N. Valmispild, C. Dutreix, M. Eckstein, M. I. Katsnelson, A. I. Lichtenstein, and E. A. Stepanov, Dynamically induced doublon repulsion in the Fermi-Hubbard model probed by a single-particle density of states, Phys. Rev. B **102**, 220301(R) (2020).
[65] N. Strohmaier, D. Greif, R. Jördens, L. Tarruell, H. Moritz, T. Esslinger, R. Sensarma, D. Pekker, E. Altman, and E. Demler, Observation of elastic doublon decay in the Fermi-Hubbard model, Phys. Rev. Lett. **104**, 080401 (2010).
[66] A. Rapp, S. Mandt, and A. Rosch, Equilibration Rates and Negative Absolute Temperatures for Ultracold Atoms in Optical Lattices, Phys. Rev. Lett. **105**, 220405 (2010).
[67] A. Rapp, Mean-field dynamics to negative absolute temperatures in the Bose-Hubbard model, Phys. Rev. A **87**, 043611 (2013).
[68] J. M. Deutsch, Eigenstate thermalization hypothesis, Rep. Prog. Phys. **81**, 082001 (2018).

[69] K. Buchta, Ö. Legeza, E. Szirmai, and J. Sólyom, Mott transition and dimerization in the one-dimensional SU(N) Hubbard model, Phys. Rev. B **75**, 155108 (2007).

[70] P. Corboz, M. Lajkó, A. M. Läuchli, K. Penc, and F. Mila, Spin-Orbital Quantum Liquid on the Honeycomb Lattice, Phys. Rev. X **2**, 041013 (2012).

[71] P. Calabrese and J. Cardy, Entanglement entropy and conformal field theory, J. Phys. A: Math. Theor. **42**, 504005 (2009).

[72] T. Zhou and A. Nahum, Entanglement Membrane in Chaotic Many-Body Systems, Phys. Rev. X **10**, 031066 (2020).

[73] E. Altman, E. Demler, and M. D. Lukin, Probing many-body states of ultracold atoms via noise correlations, Phys. Rev. A **70**, 013603 (2004).

[74] S. Gopalakrishnan, D. A. Huse, V. Khemani, and R. Vasseur, Hydrodynamics of operator spreading and quasiparticle diffusion in interacting integrable systems, Phys. Rev. B **98**, 220303(R) (2018).

[75] M. Ljubotina, M. Žnidarič, and T. Prosen, Kardar-Parisi-Zhang Physics in the Quantum Heisenberg Magnet, Phys. Rev. Lett. **122**, 210602 (2019).

[76] M. K. Joshi, F. Kranzl, A. Schuckert, I. Lovas, C. Maier, R. Blatt, M. Knap, and C. F. Roos, Observing emergent hydrodynamics in a long-range quantum magnet, Science **376**, 720 (2022).

[77] D. Wei, A. Rubio-Abadal, B. Ye, F. Machado, J. Kemp, K. Srakaew, S. Hollerith, J. Rui, S. Gopalakrishnan, N. Y. Yao *et al.*, Quantum gas microscopy of Kardar-Parisi-Zhang superdiffusion, Science **376**, 716 (2022).

[78] C. P. Moca, M. A. Werner, A. Valli, G. Zaránd, and T. Prosen, Kardar-Parisi-Zhang scaling in the Hubbard model, arXiv:2306.11540.

[79] A. Adams, L. D. Carr, T. Schäfer, P. Steinberg, and J. E. Thomas, Strongly correlated quantum fluids: Ultracold quantum gases, quantum chromodynamic plasmas and holographic duality, New J. Phys. **14**, 115009 (2012).

[80] M. Fava, B. Ware, S. Gopalakrishnan, R. Vasseur, and S. A. Parameswaran, Spin crossovers and superdiffusion in the one-dimensional Hubbard model, Phys. Rev. B **102**, 115121 (2020).

[81] A. J. Daley, J. M. Taylor, S. Diehl, M. Baranov, and P. Zoller, Atomic Three-Body Loss as a Dynamical Three-Body Interaction, Phys. Rev. Lett. **102**, 040402 (2009).

[82] X.-Y. Chen, M. Duda, A. Schindewolf, R. Bause, I. Bloch, and X.-Y. Luo, Suppression of Unitary Three-Body Loss in a Degenerate Bose-Fermi Mixture, Phys. Rev. Lett. **128**, 153401 (2022).

[83] U. Schneider, L. Hackermuller, S. Will, T. Best, I. Bloch, T. A. Costi, R. Helmes, D. Rasch, and A. Rosch, Metallic and insulating phases of repulsively interacting fermions in a 3D optical lattice, Science **322**, 1520 (2008).

[84] S.-A. Cheong and C. L. Henley, Exact ground states and correlation functions of chain and ladder models of interacting hardcore bosons or spinless fermions, Phys. Rev. B **80**, 165124 (2009).

[85] A. H. MacDonald, S. M. Girvin, and D. Yoshioka, $\frac{t}{U}$ expansion for the Hubbard model, Phys. Rev. B **37**, 9753 (1988).

[86] X. Cai, H. Yang, H.-L. Shi, C. Lee, N. Andrei, and X.-W. Guan, Multiparticle Quantum Walks and Fisher Information in One-Dimensional Lattices, Phys. Rev. Lett. **127**, 100406 (2021).